Taylor & Francis
Taylor & Francis Group

Phase Transitions
A Multinational Journal

ISSN: (Print) (Online) Journal homepage: https://www.tandfonline.com/loi/gpht20

Structural, dielectric and piezoelectric characterization of BFN-modified PZT-based (MPB) ceramics

Kahoul Fares, Benseghir Sabrina, Hamzioui Louanes, Guemache Abderrezak, Aillerie Michel & Boutarfaia Ahmed

To cite this article: Kahoul Fares, Benseghir Sabrina, Hamzioui Louanes, Guemache Abderrezak, Aillerie Michel & Boutarfaia Ahmed (2023): Structural, dielectric and piezoelectric characterization of BFN-modified PZT-based (MPB) ceramics, Phase Transitions, DOI: 10.1080/01411594.2023.2175676

To link to this article: https://doi.org/10.1080/01411594.2023.2175676

Published online: 08 Feb 2023.

PHASE TRANSITIONS
https://doi.org/10.1080/01411594.2023.2175676

Taylor & Francis
Taylor & Francis Group

Structural, dielectric and piezoelectric characterization of BFN-modified PZT-based (MPB) ceramics

Kahoul Fares[a,b], Benseghir Sabrina[a], Hamzioui Louanes[a,b], Guemache Abderrezak[a], Aillerie Michel[c,d] and Boutarfaia Ahmed[b]

[a]Département Socle Commun ST, Faculté de Technologie, Université de M'Sila, M'Sila, Algérie; [b]Laboratoire de Chimie Appliquée, Département de Chimie, Université de Biskra, Biskra, Algérie; [c]LMOPS, Université de Lorraine, Metz, France; [d]LMOPS, Centrale Supelec, Metz, France

ABSTRACT

The solid solution of $xBi(Fe_{1/3}Nb_{2/3})O_3$–(1-x)$Pb(Zr_{0.50}Ti_{0.50})O_3$ ceramics near morphotropic phase boundary (MPB) (BFN–PZT, x = 0, 0.0025, 0.005, 0.0075, 0.01) were prepared by conventional solid-state reaction method. The samples added with different Bi_2O_3, Fe_2O_3, Nb_2O_5 contents were compared in terms of the phase structure, microstructure, dielectric properties, and piezoelectric properties. In particular, rhombohedral-tetragonal morphotropic phase boundary was observed in BFN–PZT crystal structure near the composition of x = 0.005. The BFN–PZT ceramics exhibited the following optimal properties at x = 0.005: dielectric constant ε_r of 847, dielectric loss tanδ of 0.034, Curie temperature T_C of 390°C, electrical conductivity σ of 0.441 $(Mohm.m)^{-1}$, piezoelectric charge constant d_{33} of 416 pC/N, electromechanical coupling factor K_P of 0.654, and mechanical quality factor Q_m of 426, making it a promising material for use in high-intensity ultrasound applications.

ARTICLE HISTORY
Received 2 September 2022
Accepted 30 January 2023

KEYWORDS
MPB; piezoelectric ceramics; solid-state reaction; domain structure; PZT

1. Introduction

The $Pb(Zr_{1-x}Ti_x)O_3$-based ceramics are extensively used in high-end piezoelectric sensors, transducers, actuators, electronic devices, and piezoelectric transformers due to their excellent dielectric, energy storage, piezoelectric, ferroelectric, and optoelectronic properties [1–3]. In the perovskite structure (ABO_3) of ferroelectric PZT, the Pb^{2+} occupies the A-site and Ti^{4+} or Zr^{4+} the B-site. Further enhancement in the properties of such ferroelectric ceramics will also enhance the performance of these devices. This has therefore become an interesting subject of research among material scientists over the past few decades [1]. All these devices require piezoelectric ceramic materials with a high Curie temperature, excellent piezoelectric properties and good temperature stability to ensure stable operation under high temperature conditions. With high Curie temperature and outstanding piezoelectric properties, bismuth ferrite-barium titanate ($BiFeO_3$-$BaTiO_3$, BF-BT), potassium sodium niobate (($K_{0.5}Na_{0.5}$) NbO_3, KNN), lead bismuth scandium titanate ($BiScO_3$-$PbTiO_3$, BS-PT) and lead zirconate titanate ($PbZrO_3$-$PbTiO_3$, PZT) etc. are expected to show their talents in the application of high-temperature piezoelectric devices [4].

It is generally believed that the morphotropic phase boundary (MPB (at which a transition occurs between rhombohedral (Zr-rich side) and tetragonal phases (Ti-rich side))), nano-domain, and local structural heterogeneity are important factors to generate a high piezoelectric response. From a thermodynamic perspective, when the composition is close to the MPB, the curvature of the free energy

CONTACT Kahoul Fares Fares.kahoul@univ-msila.dz

curve decreases with the polarization vector when in a stable state, indicating that spontaneous polarization is more likely to rotate under an external field [4, 5]. The doping ions introduce local structural heterogeneity at the nanoscale, which changes the thermodynamic energy distribution [6, 7].

Small amounts of foreigner doping ions may be incorporated in the PZT composition to alter its electrical, piezoelectric, and ferroelectric properties. To enhance the electrical and electromechanical properties of the materials greatly, various kinds of modifications can be made by suitable substitutions at A(Pb) or B(Zr/Ti) sites of PZT ceramics [8–13].

The substituents in the PZT system were classified into 'softeners' and 'hardeners' to attain specific physical properties [14, 15]. The substituents like Sm^{3+}, Bi^{3+}, and La^{3+} donor ions (at A-site) and Nb^{5+}, Sb^{5+} ions (at B-site) create A-site vacancies in the lattice and are called 'softeners' [16–22]. The dopants like Na^{+}, K^{+} acceptor ions (at A-site), and Mn^{3+}, Fe^{3+}, Al^{3+} ions (at B-site) can create oxygen vacancies in the lattice and can be called 'hardeners' [17, 18, 21, 23].

In this paper, we prepared $xBi(Fe_{1/3}Nb_{2/3})O_3$–$(1\text{-}x)Pb(Zr_{0.50}Ti_{0.50})O_3$ (BFN–PZT) piezoceramics sintered at 1100°C temperature by the traditional solid-reaction method. The effect of various content Bi^{3+}, Fe^{3+} and Nb^{5+} ions on the phase formation, crystal structure and surface morphology in BFN–PZT ceramics were systematically investigated. Further, dielectric, piezoelectric properties and electrical conductivity of BFN–PZT ceramics have been explored within the range of frequencies and temperature.

2. Experimental procedure

The BFN–PZT piezoceramics were fabricated via the solid-state reaction route. The starting powders were reagent grade Bi_2O_3 (99.9%), Fe_2O_3 (99.6%), Nb_2O_5 (99.5%), PbO (99%), ZrO_2 (99%), and TiO_2 (99%). According to the stoichiometric ratios of the formula $xBi(Fe_{1/3}Nb_{2/3})O_3$–$(1\text{-}x)Pb(Zr_{0.50}Ti_{0.50})O_3$ (x = 0, 0.0025, 0.005, 0.0075 and 0.01), the powders were weighed and an excess of 2 wt% PbO was added to all compositions to compensate for the partial evaporation of PbO at the high temperatures required for sintering. After weighing, the raw powders were mixed by ball milling in ethanol for 24 h. The mixed powders were dried and then calcined at 900°C for 3 h with a heating rate of 5°C/min. The calcined clinker was ground to powders with a mortar and then the powders were ball milled again for 24 h. The 5% polyvinyl alcohol (PVA) solution was added to the calcined powders. The discs with a diameter of 10 mm and a thickness of 1 mm were pressed under the uniaxial pressure of 100 MPa. The green pellets were burnt out at 550°C for 2 h to remove the PVA binder and then sintered at 1100°C for 3 h in a sealed alumina crucible. The silver paste was screen-printed on the surfaces of the sintered pellets and then fired at 750°C for 10 min. The samples with silver electrodes were poled in silicone oil at 120°C for 45 min under a DC voltage of 40 kV/cm.

The phase analysis of the samples (ground into powders) was carried out using X-Ray diffraction (XRD) with CuKα radiation (X'Pert Pro MPD instrument, B.V. PANalytical, Netherlands). The sample surface morphology was observed using a cold-field emission high resolution scanning electron microscope (JSM7500F, JEOL Japan). Dielectric properties were obtained by measuring the temperature dependence of the capacitance and phase angle (HIOKI 3532). The piezoelectric constant (d_{33}) was measured using a quasi-static piezoelectric d_{33} meter (Model ZJ-3A, Institute of Acoustics, Chinese Academy of Science). The electromechanical coupling coefficient (K_P) and mechanical quality factor (Q_m) were determined using an impedance analyzer (model HP4294A, Agilent, USA) according to the IEEE standard through resonance and anti-resonance technology.

3. Results and discussion

3.1. X-ray diffraction analysis

Figure 1 shows the room temperature XRD patterns in the 2θ range from 20° to 60° for the $xBi(Fe_{1/3}Nb_{2/3})O_3$–$(1\text{-}x)Pb(Zr_{0.50}Ti_{0.50})O_3$ ceramics sintered at 1100°C with different BFN contents (x = 0,

0.0025, 0.005, 0.0075 and 0.01). All samples showed typical diffraction peaks of perovskite structure, and no secondary phase was observed, implying that Bi, Fe, and Nb atoms dissolved into the BFN–PZT lattice and formed a homogeneous solid solution.

It is apparent from the XRD patterns from 43° to 47° (Figure 1) which clearly reveal a phase transformation from the tetragonal structure to the rhombohedral structure with an increase in x. The samples with x = 0 and 0.0025 exhibited tetragonal structure characterized by a peaks $(0\ 0\ 2)_T$ and $(2\ 0\ 0)_T$. Then, the $(0\ 0\ 2)_T$ and $(2\ 0\ 0)_T$ reflection obviously broadened and could clearly be fit using three peaks: $(002)_T$, $(200)_T$, and $(200)_R$. These results can be attributed to the well-known morphotropic phase boundary (MPB), where two ferroelectric phases (tetragonal and rhombohedral) coexist [24]. The ceramics exist as rhombohedral phase with x = 0.0075 and 0.01, as indicated by the splitting of the $(200)_R$ peak in the 2θ range from 43° to 47°. The ceramics in the x = 0.005 coexisted as tetragonal and rhombohedral phases, as revealed by the coexistence of $(002)_T$, $(200)_T$, and $(200)_R$ peaks. Therefore, it can be asserted that the composition with x = 0.005 is close to the MPB of this system.

Due to the similar radii of Fe^{3+} (0.064 nm), Ti^{4+} (0.0605 nm), Zr^{4+} (0.072 nm), and Nb^{5+} (0.064 nm) at the octahedral sites of the perovskite lattice, forming additional anionic vacancies, the phenomenon can be explained by penetration of Fe^{3+} and Nb^{5+} ions into the grains to substitute for B-site ions, causing lattice distortion [1]. The smaller ionic radius of Bi^{3+} (0.103 nm), compared to that of Pb^{2+} (0.119 nm) promotes the phase transformation from tetragonal to rhombohedral [16].

The fraction of the tetragonal phase (F_T) or rhombohedral phase (F_R) in the perovskite structure was calculated using the following equation:

$$F_T = \frac{I^T_{(002)} + I^T_{(200)}}{I^T_{(002)} + I^T_{(200)} + I^R_{(200)}}$$

$$F_R = 1 - F_T$$

Where $I^T_{(002)}$ and $I^T_{(200)}$ are the area of the fitted Gaussian function for the (002) and (200) tetragonal reflection peaks, respectively; and $I^R_{(200)}$ is the area of simulated Gaussian function for the

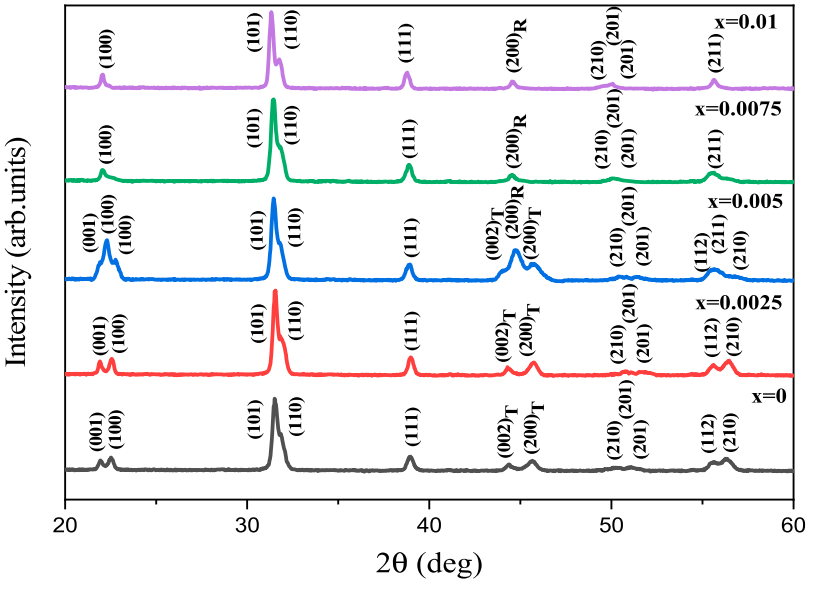

Figure 1. XRD of sintered powders of $xBi(Fe_{1/3}Nb_{2/3})O_3$–$(1-x)Pb(Zr_{0.50}Ti_{0.50})O_3$ ceramics with x = 0, 0.0025, 0.005, 0.0075 and 0.01.

(200) rhombohedral reflection peak. Using the above equation, the fraction values of both the tetragonal phase and the rhombohedral phases for PMSZNZT-100x specimens with different x contents in the integrated angle range. The above-mentioned integrated angle range is set by calculating two standard deviation of fitted Gaussian function. The fraction of rhombohedral phase (F_R %) for the various studied systems have been summarized in Table 1.

3.2. SEM morphology

Figure 2(a–e) show SEM images for the BFN–PZT ceramics with different BFN contents. As can be seen from the images, all samples show a uniform grain shape. It can be seen that the grain size of BFN–PZT at the MPB is slightly larger than that at T and R. No pyramidal grains were observed, indicating the absence of undesirable pyrochlore phases, which validates the XRD results, reported above. The substitution of Pb^{2+} ions with smaller Bi^{3+} ions makes Bi^{3+} more easily enter the lattice, leading to shrinkage of the oxygen octahedron, lattice distortion, and mass transport, thus promoting grain growth.

The larger average grain size means a smaller grain boundary, which is beneficial for mass transport and domain rotation, thus enhancing the electrical properties [25–27].

3.3. Dielectric properties

The temperature-dependent studies of dielectric constant (ε_r) of BFN-modified PZT ceramics are shown in Figure 3. The temperature was varied from room temperature to 450°C. The dielectric constant (ε_r) of all ceramics initially increased and then decreased as the temperature increased. The temperature corresponding to the peak the dielectric constant is called the Curie temperature (T_C). At T_C, the appearance of peaks indicates the phase transition of the compounds from the ferroelectric phase to paraelectric phase [28, 29]. The value of ε_r at T_C is known as maximum dielectric permittivity (ε_{max}). From Figure 3, it is also evident that the value of ε_r increases up to x = 0.005 and thereafter start to decrease. The specimen having composition x = 0.005 shows maximum value of dielectric constant which is 8178 near T_C. Additionally, the substitution of BFN into PZT matrix slightly increases the transition temperature from 370°C (x = 0) to 390°C (x = 0.005) which is quite high and may be useful in technical applications. The reason for the improvement in dielectric properties and deterioration in microstructural for the composition x = 0.005 may be attributed to the fact that the composition is very close to the morphotropic phase boundary (MPB) [30, 31].

It is well known that diffusion phase transition characteristics are directly associated with the formation of point defects after doping. The ionic radius of Fe^{3+} (0.064 nm) and Nb^{5+} (0.064 nm) ions is similar to those of B-site atoms, such as Zr^{4+} (0.072 nm), Ti^{4+} (0.0605 nm), and the ionic radius of Bi^{3+} ions (0.103 nm) is similar to that of A-site Pb^{2+} atoms (0.119 nm) [3, 32]. Hence, the BFN doped BFN–PZT ceramic samples exhibited a high disorder due to the diffused paraelectric–ferroelectric phase transition caused by relaxor characteristics.

The temperature dependence of dielectric loss (tanδ) at 1 kHz of BFN–PZT ceramics is shown in Figure 4. Only a dielectric loss anomaly (T_C) corresponding to the ferroelectric phase to paraelectric cubic phase can be observed in tanδ-T curves for all samples.

Figure 5(a,b) shows the frequency dependence of the ε_r and tanδ values of BFN–PZT ceramics measured at room temperature. Both ε_r and tanδ magnitude of the entire prepared sample, is reduced with increase in frequency, confirming again the characteristic dielectric nature of the compounds. One sees that the magnitude of room temperature ε_r is higher and lower at low and high

Table 1. Fraction of rhombohedral phase of BFN–PZT ceramics.

x	0	0.0025	0.005	0.0075	0.01
F_R (%)	28.13	32.33	48.81	67.86	72.46

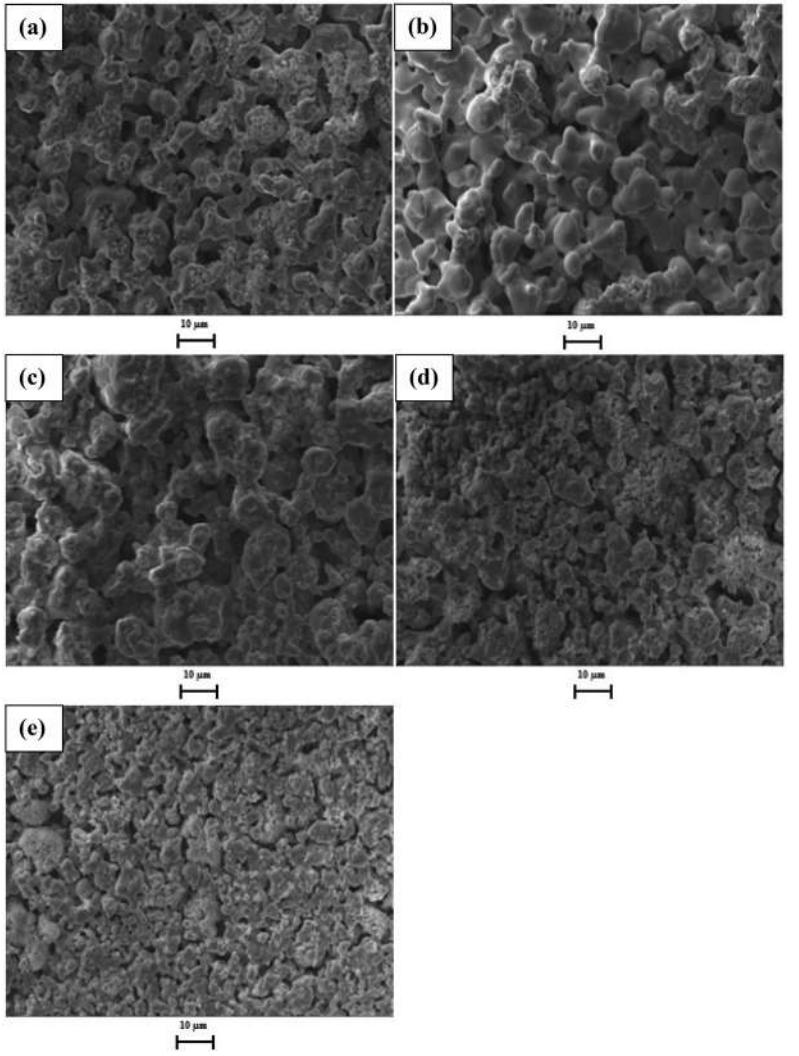

Figure 2. SEM images for the BFN–PZT piezoceramics with different compositions: (a) x = 0, (b) x = 0.0025, (c) x = 0.005, (d) x = 0.0075, and (e) x = 0.01.

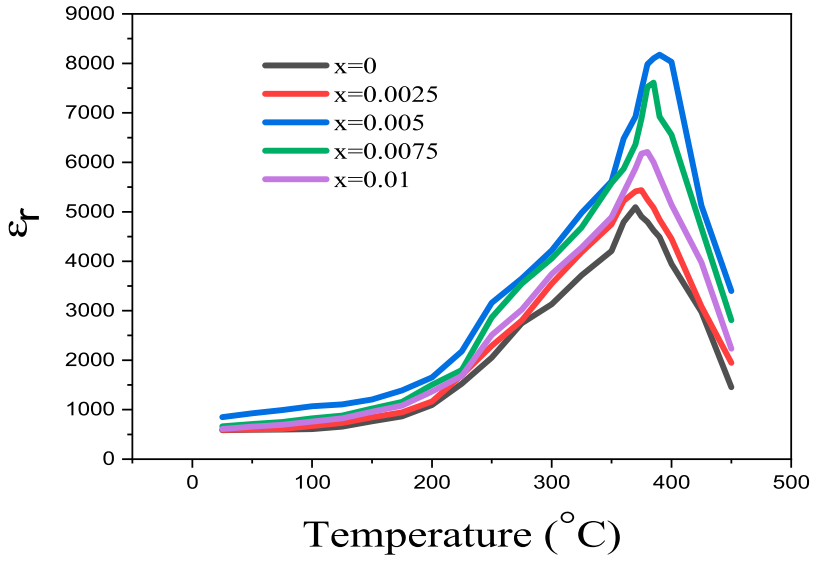

Figure 3. Temperature-dependent dielectric constant of all samples BFN–PZT at 1 kHz.

frequencies respectively. This represents the contribution of all the respective dielectric polarizations and only electronic polarization to ε_r at low and high frequencies respectively. Smooth decrease of tanδ of ceramics with rise in frequency is due to the relatively large packing fraction of the compounds because the loss mainly results from scattering phenomenon [29]. The cross sections of scattering rely up on grain size and grain boundaries. Small grain size increases the scattering amplitude [29].

Figure 6 exhibits the dielectric permittivity (ε_r), Curie temperature (T_C) and dielectric loss (tanδ) for the BFN–PZT piezoceramics with different BFN substituting amounts measured at 1 kHz and

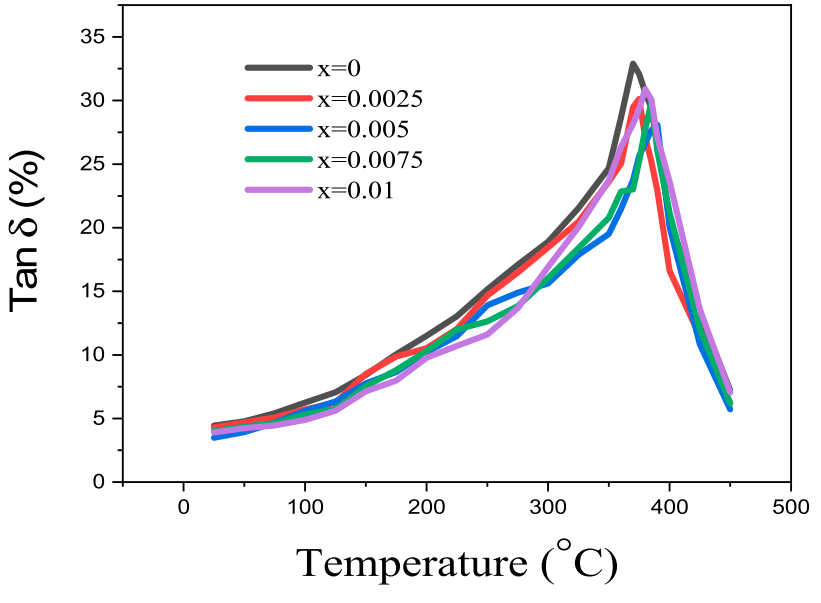

Figure 4. Temperature-dependent dielectric loss of all samples BFN–PZT at 1 kHz.

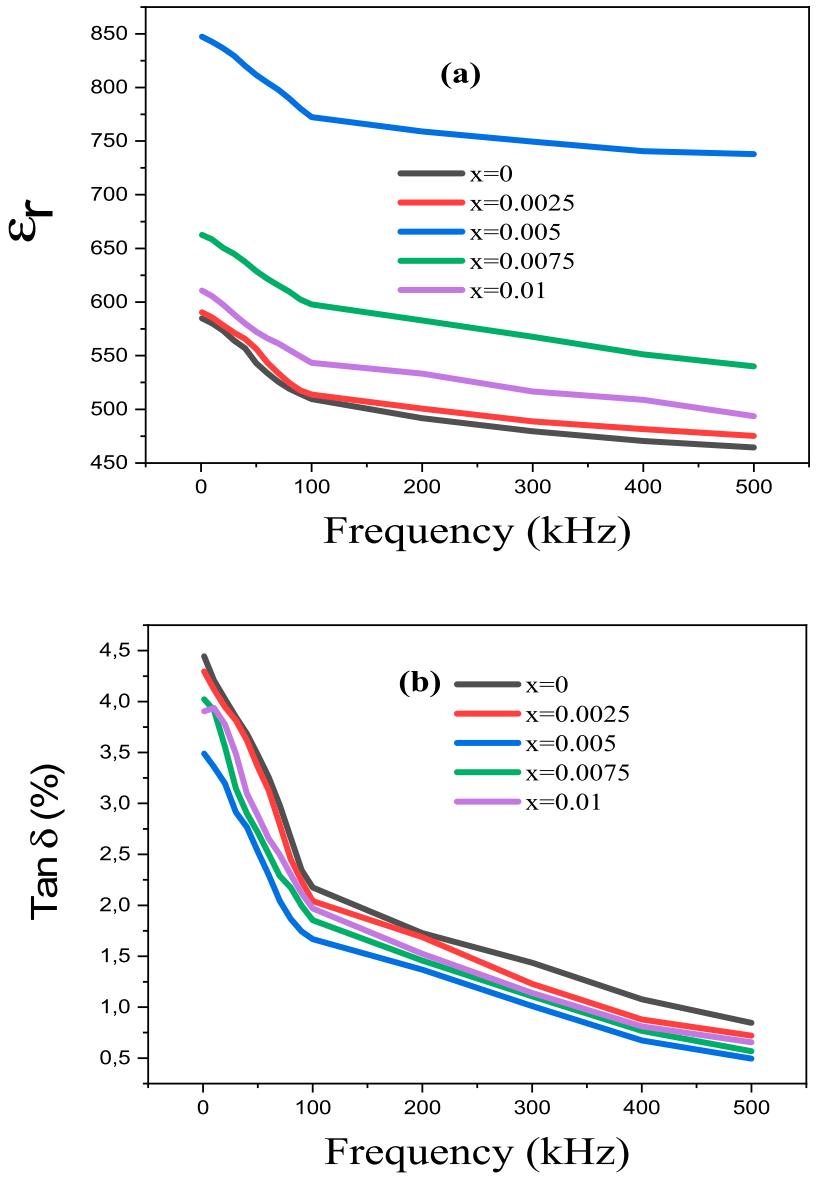

Figure 5. Variation of ε_r (a) and tanδ (b) of BFN–PZT ceramics with frequency.

25°C. The ε_r sharply increases from 585 with x = 0 to a maximum of 847 with x = 0.005, and then gradually decreases to 611 with x = 0.01. The T_C increases from 370°C with x = 0–390°C with x = 0.005 then fluctuates slightly (decreases). The tanδ reduces from 0.0444 with x = 0–0.0348 with x = 0.005 and then increases. The enhancement of the dielectric permittivity may be due to the A-site substitution of the Bi^{3+} for Pb^{2+} ions, which causes lattice distortion and promotes domain wall movement [27, 33].

It is difficult to describe the motion of charge carriers in ceramic materials because various complex dynamic processes are involved. However, conductivity can be described as an acceptable way for the electrical properties of the studied materials. It is well known that PZT ceramics possesses p-type conductivity (hole-type conduction), caused by Pb loss due to high volatility of PbO during the sintering process [15, 34, 35]. Figure 7 show the plot of electrical conductivity (σ)

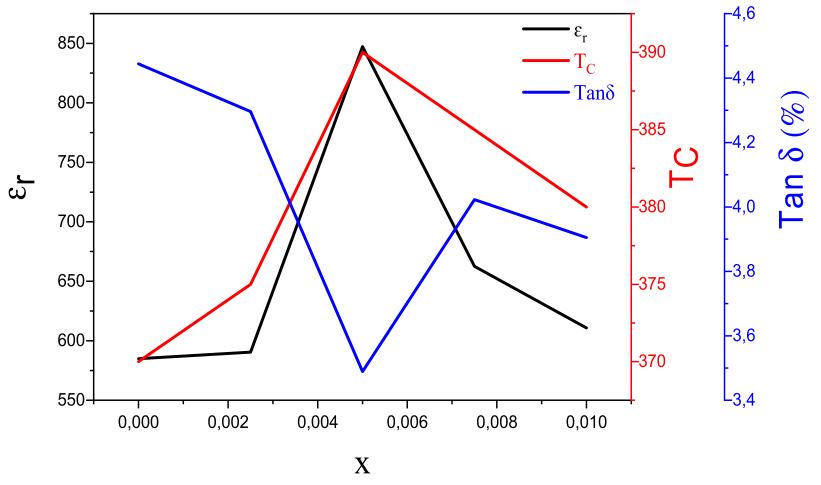

Figure 6. Dielectric permittivity (ε_r), Curie temperature (T_C) and dielectric loss (tanδ) for the ceramics as a function of x values measured at 1 kHz and 25°C.

of BFN–PZT for different concentrations of BFN (x = 0, 0.0025, 0.005, 0.0075 and 0.01) at different temperatures.

It can be seen that all the compositions exhibited a increase in conductivity with the increase in temperature, which indicates a negative temperature coefficient of resistance (NTCR) [36]. Generally, oxygen vacancies will be created by the low valence ions, which can enter the lattice site. Once these vacancies are increased, the substituted ions behave as acceptors and holes, contribute to the conduction process. Excess dopant contribution may produce either A-site (Pb) or oxygen vacancies [36, 37]. After increasing lead vacancies, bismuth will be a donor and contribute electrons

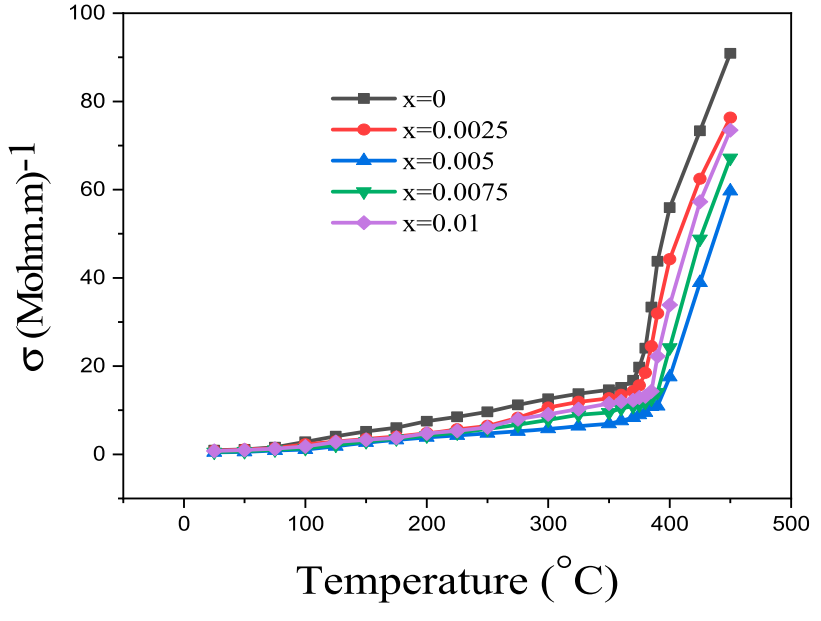

Figure 7. Variation of electrical conductivity with temperature for $xBi(Fe_{1/3}Nb_{2/3})O_3$–$(1-x)Pb(Zr_{0.50}Ti_{0.50})O_3$ ceramics at frequency of 1 kHz.

to the conduction mechanism. At high temperatures, the conductivity was increased and specifies that extra charge carriers can be produced due to donor contribution.

3.4. Piezoelectric characterization

The temperature stability of piezoelectric properties of ceramics is an important index for high-temperature applications of piezoelectric ceramics. Therefore, this work evaluates the piezoelectric properties stability of high-temperature poled BFN–PZT ceramics.

Figure 8 shows the temperature dependence of piezoelectric charge constant (d_{33}) values of poled ceramics at different temperatures from 25 to 450°C. The d_{33} of BFN–PZT ceramics remains stable before Curie temperature. When the temperature is close to Curie temperature, the d_{33} of BFN–PZT ceramics decreases abruptly, and the ceramics are depolarized. The samples can be used sustainably (good temperature stability) to 390°C and the change rate of d_{33} from 25 to 390°C is only 2%.

The temperature dependence of K_P and Q_m of BFN–PZT ceramics with a temperature change from 25 to 450°C are shown in Figure 9. The K_P and Q_m of BFN–PZT ceramics keep stable with increasing temperature initially, and then tend to zero when the temperature is near the T_C. The defect dipoles on domain walls can act as pinning points which prevent the domain from movement and hence decrease the K_P and Q_m value. Another possible reason for the decrease in electromechanical coupling factor and mechanical quality factor with increasing temperature can be possibly explained using volume theory, where the degree of decrease is considered partly due to a gradual alignment of a doubly positively charged oxygen vacancy associated with defect dipoles in the perovskite lattice [38, 39].

Figure 10 displays the piezoelectric properties for the BFN–PZT ceramics with the different BFN content. As shown in Figure 10, both K_P and d_{33} exhibit similar changing trends with the increased BFN amount. The sample with x = 0.005 BFN content has both K_P and d_{33} up to the maximum of 0.654 and 416 pC/N, respectively. However, the mechanical quality factor (Q_m) has an opposite changing trend to that of the d_{33} or K_P.

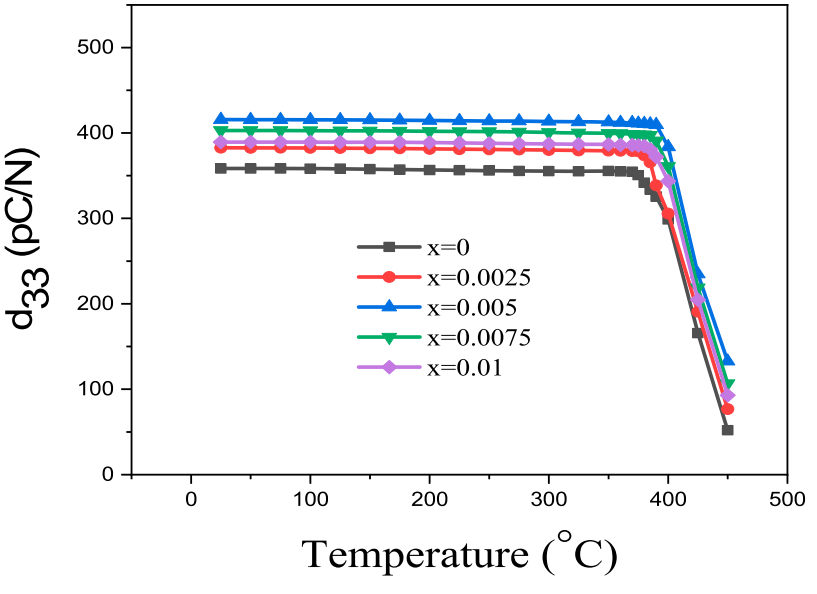

Figure 8. Piezoelectric charge constant (d_{33}) as a function of de temperature of BFN–PZT ceramics.

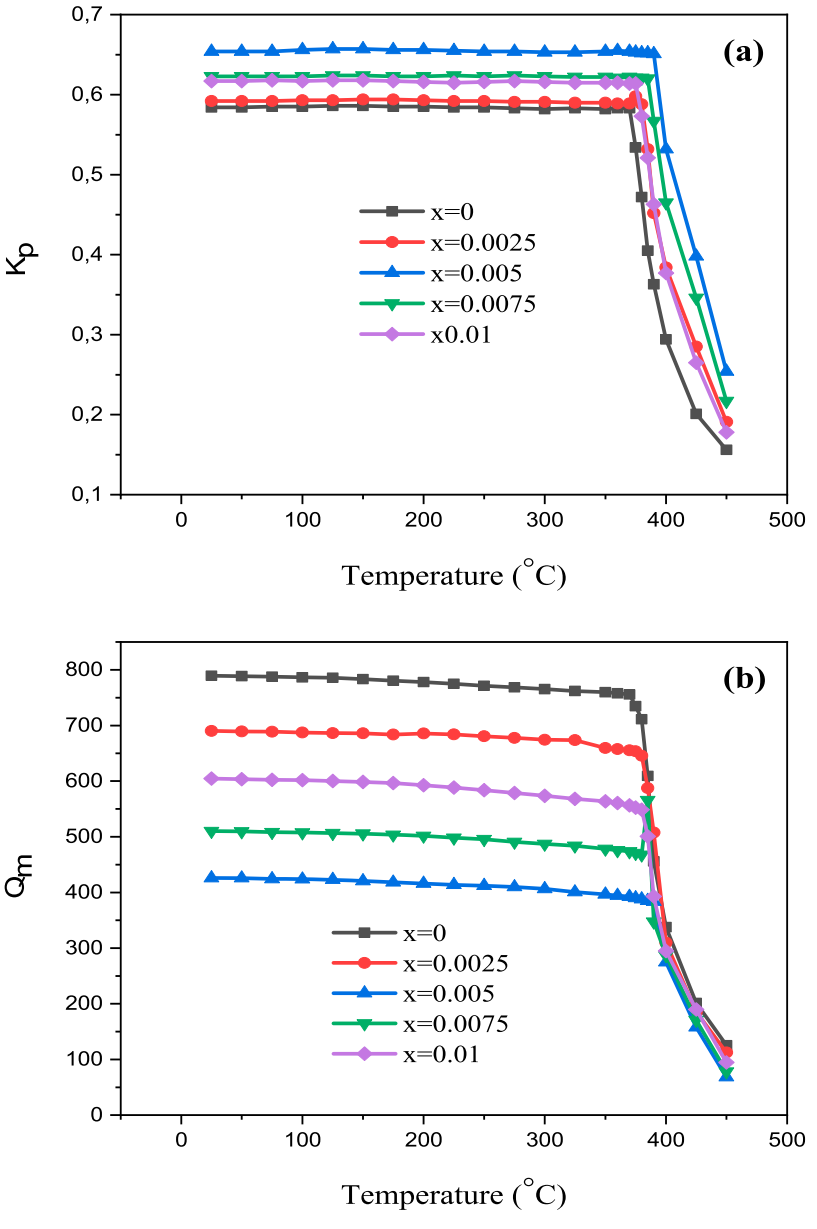

Figure 9. Temperature dependence of K_P (a) and Q_m (b) of the BFN–PZT ceramics sintered at 1100°C with various BFN contents.

These results are probably related to the increased grain size and the morphotropic phase boundary effect [1, 40–42]. The two phases coexist at the MPB, so the spontaneous polarization can point along any 1 of 14 directions, and the activation energy for domain motion is too low, allowing even very weak electric fields to induce changes in the spontaneous polarization [42, 43].

The fact that the substitution of Bi^{3+} ions for Pb^{2+} ions at the A-site leads to lattice distortion and the promotion of domain wall movement, which is beneficial to the improvement of the piezoelectric response [27, 33]. In addition, the d_{33} and K_P have the same changing trends as the average grain size increases. The clamping effect of the grain boundary on the domain wall motion greatly reduces due to the increased grain size with x from 0 to 0.005, which enhances the piezoelectric

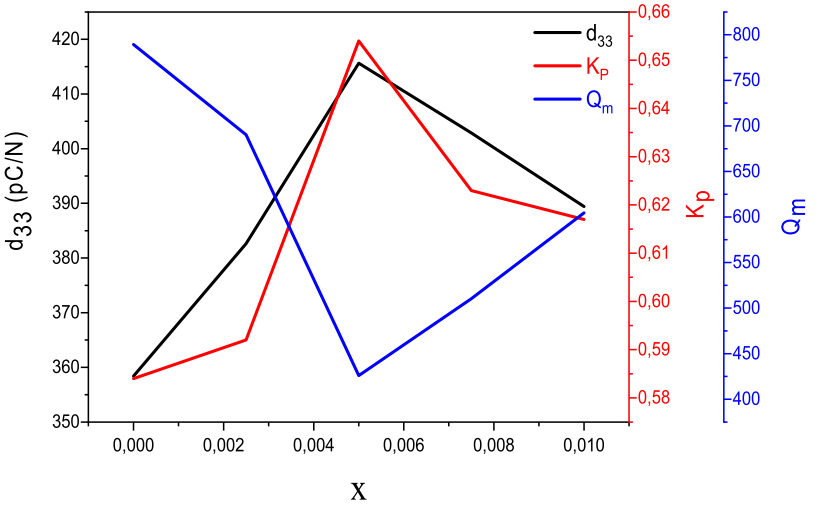

Figure 10. d_{33}, K_P, and Q_m as functions of BFN content measured at room temperature.

Table 2. Comparison of physical properties of BFN-PZT ceramics with similar PZT ceramics at room temperature (1 kHz).

	ε_r	tanδ (%)	σ (Mohm.m)$^{-1}$	K_P	Q_m	d_{33} (pC/N)	Reference
PZT	585	4.444	0.935	0.584	789	358	This work
0.0025 BFN–0.9975 PZT	590	4.296	0.815	0.592	690	383	This work
0.005 BFN–0.995 PZT	847	3.489	0.441	0.654	426	416	This work
0.0075 BFN–0.9925 PZT	663	4.023	0.535	0.623	510	403	This work
0.01 BFN–0.99 PZT	611	3.905	0.774	0.617	605	389	This work
PZT-PZMnN	1281	0.500	–	0.610	1260	340	[3]
PYBZT-PMS	1119	1.530	0.709	0.639	525	–	[16]
PZT-SFN	1009	1.110	–	0.661	473	–	[17]
PMS-PZT-Ce-Yb-xFe	1055	0.295	–	0.61	1500	360	[32]
PZT-YTS	714	3.345	0.873	0.635	622	–	[35]

properties [44]. With x increasing from 0.005–0.01, the average grain size gradually decreases, and more grain boundaries between the small grains inhibit the domain rotation and the domain wall movement, resulting in the deterioration of the electrical properties [45–47].

Table 2 lists dielectric and piezoelectric properties of BFN-PZT ceramics comparable to similar PZT ceramics as published in recent years.

4. Conclusions

In this paper, we have presented the synthesis of series of excessively Bi_2O_3, Fe_2O_3, and Nb_2O_5 substituted BFN–PZT ceramics by a conventional solid-state reaction method. The used chemical formula for the synthesis was $xBi(Fe_{1/3}Nb_{2/3})O_3$–$(1\text{-}x)Pb(Zr_{0.50}Ti_{0.50})O_3$ wih x = 0, 0.0025, 0.005, 0.0075 and 0.01. The effect of excessive Bi^{3+} doping at Pb-site, and Fe^{3+}, Nb^{5+} doping at Zr/Ti-site on the structural and electrical properties was reported. The structure of all ceramics sintered at 1100°C showed pure perovskite structure, which transformed from tetragonal to rhombohedral phase as the BFN content was increased. The oxygen vacancies facilitate mass transport, which promotes the sinterability and induces the grains to grow. The optimal electrical properties with $d_{33} = 416$ pC/N, $K_P = 0.654$, $Q_m = 426$, $\varepsilon_r = 847$, tanδ = 0.034 and $T_C = 390$°C can be observed in BFN–PZT sample with x = 0.005. Thus, the ceramics synthesized in this study provide a strong basis for potential applications in high-intensity ultrasound applications [48].

Disclosure statement

No potential conflict of interest was reported by the author(s).

References

[1] Vuong LD, Gio PD, Quang NDV, et al. Development of $0.8Pb(Zr_{0.48}Ti_{0.52})O_3$–$0.2Pb[(Zn_{1/3}Nb_{2/3})_{0.625}$-$(Mn_{1/3}Nb_{2/3})_{0.375}]O_3$ ceramics for high-intensity ultrasound applications. J Electron Mater. 2018;47:5944–5951.

[2] Zhang J, Zhang Y, Yan Z, et al. Fabrication and performance of PNN-PZT piezoelectric ceramics obtained by low-temperature sintering. Sci Eng Compos Mater. 2020;27:359–365.

[3] Vuong LD. Densification behavior and electrical properties of the PZT-PZMnN-based ceramics prepared by two-step sintering. J Mater Sci Mater Electron. 2022;33:6710–6721.

[4] Damjanovic D. Comments on origins of enhanced piezoelectric properties in ferroelectrics. IEEE Trans Ultrason Ferroelectr Freq Control. 2009;56:1574–1585.

[5] Fu HX, Cohen RE. Polarization rotation mechanism for ultrahigh electromechanical response in single-crystal piezoelectrics. Nature. 2000;403:281–283.

[6] Li F, Lin DB, Chen ZB, et al. Ultrahigh piezoelectricity in ferroelectric ceramics by design. Nature Mater. 2018;17:349–354.

[7] Pu T, Chen H, Xing J, et al. High piezoelectricity of low-temperature sintered Li_2CO_3-added PNN–PZT relaxor ferroelectrics. J Mater Sci Mater Electron. 2022;33:4819–4830.

[8] Ranjan R, Kumar R, Kumar N, et al. Impedance and electric modulus analysis of Sm-modified $Pb(Zr_{0.55}Ti_{0.45})_{1-x/4}O_3$ ceramics. J Alloys Compd. 2011;509:6388–6394.

[9] Rema KP, Etacheri VK, Kumar V. Influence of low trivalent iron doping on the electrical characteristics of PZT. J Mater Sci Mater Electron. 2010;21:1149–1153.

[10] Ye ZG, Toda K, Sato M. Synthesis structure and properties of the magnetic relaxor ferroelectric $Pb(Fe_{2/3}W_{1/3})O_3$ [PFW]. J Kor Phys Soc. 1998;32:S1028–S1031.

[11] Sukla AK, Agrawal VK, Das IML, et al. Dielectric response of PLZT ceramics x/57/43 across ferroelectric– para-electric phase transition. Bull Mater Sci. 2011;34:133–142.

[12] Garcia JE, Ochoa DA, Gomis V, et al. Evidence of temperature dependent domain wall dynamics in hard lead zirconate titanate piezoceramics. J Appl Phys. 2012;112:014113–0141117.

[13] Panigrahi SC, Das PR, Padhee R. Electrical properties of Gd-modified PZT (MPB) ceramics. Pramana J Phys. 2021;95:70–81.

[14] Jaffe B, Cook WR, Jaffe H. Piezoelectric ceramics. London: academic press; 1971.

[15] Thomann H. Stabilization effects in piezoelectric lead titanate zirconate ceramics. Ferroelectrics. 1972;4:141–146.

[16] Benseghir S, Kahoul F, Hamzioui L, et al. Phase transition, microstructure and electrical properties of $Pb_{1-x}Y_{x/2}Bi_{x/2}[(Zr_{0.53}\ Ti_{0.47})_{0.92}$–$(Mn_{1/3}\ Sb_{2/3})_{0.08}]O_3$ piezoelectric ceramics. Ferroelectrics. 2021;584:198–211.

[17] Kahoul F, Hamzioui L, Guemache A, et al. Study of dielectric and piezoelectric properties of (1-x)PZT-xSFN ceramics prepared by conventional solid state reaction method. J Chem Soc Pak. 2020;42:634–638.

[18] Hamzioui L, Kahoul F, Guemache A, et al. Effect of Zr/Ti ratio on piezoelectric and dielectric properties of $0.1Pb[Fe_{1/2}\ Nb_{1/2}]O_3$-$0.9Pb[Zr_xTi_{(1-x)}]O_3$ ceramics. Trans Ind Ceram Soc. 2021;80:60–63.

[19] Atkin RB, Holman RL, Fulrath RM. Substitution of Bi and Nb ions in lead zirconate-titanate. J Am Ceram Soc. 1971;54:113–115.

[20] Banno H, Tsunooka T. Piezoelectric properties and temperature dependences of resonant frequency of WO_3-MnO_2-modified ceramics of $Pb(Zr\text{-}Ti)O_3$. Jpn J Appl Phys. 1967;6:954–961.

[21] Garcia JE, Perez R, Albareda A, et al. Non-linear dielectric and piezoelectric response in un-doped and Nb^{5+} or Fe^{3+} doped PZT ceramic system. J Eur Ceram Soc. 2007;27:4029–4032.

[22] Babu TA, Ramesh KV, Badapanda T, et al. Structural and electrical studies of excessively Sm_2O_3 substituted soft PZT nanoceramics. Ceram Internat. 2021;47:31294–31301.

[23] Yamashita Y, Hosono Y, Harada K, et al. Present and future of piezoelectric single crystals and the importance of the B-site cations for high piezoelectric response. IEEE Trans Ultrason Ferroelectr Freq Control. 2002;49:184–192.

[24] Qaiser MA, Hussain A, Xu Y, et al. CuO added $Pb_{0.92}Sr_{0.06}Ba_{0.02}\ (Mg_{1/3}Nb_{2/3})_{0.25}\ (Ti_{0.53}Zr_{0.47})_{0.75}O_3$ ceramics sintered with Ag electrodes at 900°C for multilayer piezoelectric actuator. Chin Phys B. 2017;26:307702–037707.

[25] Jo W, Dittmer R, Acosta M, et al. Giant electric-field-induced strains in lead free ceramics for actuator applications–status and perspective. J Electroceram. 2012;29:71–93.

[26] Randall CA, Kim N, Kucera JP, et al. Intrinsic and extrinsic size effects in fine-grained morphotropic phase boundary lead zirconate titanate ceramics. J Am Ceram Soc. 1998;81:677–688.

[27] Chen H, Pu T, Luo Y, et al. Enhancement of piezoelectric properties in low-temperature sintering PZN–PZT Ceramics by Sr^{2+} Substitution. J Electr Material. 2022;51:1261–1271.
[28] Behera B, Nayak P, Choudhary RNP. Dielectric anomaly in $LiCa_2V_5O_{15}$ ceramics. Mater Lett. 2007;61:3859–3862.
[29] Balgovind T, Babu T, Choudhary RNP. Dielectric response of Mn and Ce substituted PZT ferroelectric ceramics. Materials Today Proceedings. 2021;43:535–540.
[30] Ramam K, Chandramouli K. Dielectric and piezoelectric properties of combinatory effect of A-site isovalent and B-site acceptor doped PLZT ceramics. Ceram Silikaty. 2009;53:189–194.
[31] Kumar A, Pal V, Mishra SK. Preparation, microstructure, dielectric and electrical analysis of Fe-modified PZT piezoceramics. J Mater Sci Mater Electron. 2021;32:2946–2952.
[32] Wu QC, Hao MM, Zeng ZQ, et al. Nonlinear dielectric effect of Fe_2O_3-doped PMS–PZT piezoelectric ceramics for high-power applications. Ceram Internat. 2017;43:10866–10872.
[33] Wang CH. The piezoelectric and dielectric properties of PZT–PMN–PZN. Ceram Internat. 2004;30:605–611.
[34] Stenger CGF, Burggraaf AJ. Study of phase transitions and properties of tetragonal (Pb,La)(Zr,Ti)O3 ceramics —II: Diffuse phase transitions and thermodynamics. J Phys Chem Solids. 1980;41:25–30.
[35] Djoudi Y, Kahoul F, Hamzioui L, et al. Influence of YTS addition on structural and electrical properties of PZT-based ceramics. Process Applica Ceram. 2021;15:279–287.
[36] Kahoul F, Hamzioui L, Guemache A, et al. Phase structure, microstructure, and dielectric properties of (1–x)Pb$(Zr_{0.50}Ti_{0.50})O_3$–x$Ba(W_{2/3}Mn_{1/3})O_3$ ceramics. Ferroelectrics. 2021;572:229–237.
[37] Wu L, Wu T, Wei CC, et al. The DC resistivity of modified PZT ceramics. J Phys C Solid State Phys. 1983;16:2823–2832.
[38] Maiwa H, Kim S, Ichinose N. Temperature dependence of the electrical and electromechanical properties of lead zirconate titanate thin films. Appl Phys Lett. 2003;83:4396–4398.
[39] Basu T, Sen S, Seal A, et al. Temperature dependent electrical properties of PZT wafer. J Electron Mater. 2016;45:2252–2257.
[40] Vuong LD, Gio PD, Tho NT, et al. Relaxor ferroelectric properties of PZT-PZN-PMnN ceramics. Indian J Eng Mater Sci. 2013;20:555–560.
[41] Luan NDT, Vuong LD, Chuong TV, et al. Structure and physical properties of PZT-PMnN-PSN ceramics near the morphological phase boundary. Adv Mater Sci Eng. 2014;2014:1–8.
[42] Yuhan X. Ferroelectric materials and their applications. Amsterdam: Elsevier; 1991.
[43] Luo N, Li Q, Xia Z. Effect of $Pb(Fe_{1/2}Nb_{1/2})O_3$ modification on dielectric and piezoelectric properties of Pb$(Mg_{1/3}Nb_{2/3})O_3$–$PbZr_{0.52}Ti_{0.48}O_3$ ceramics. Mater Res Bull. 2011;46:1333–1339.
[44] Hou YD, Chang LM, Zhu MK, et al. Effect of Li_2CO_3 addition on the dielectric and piezoelectric responses in the low-temperature sintered 0.5PZN–0.5PZT system. J Appl Phys. 2007;102:084507–084513.
[45] Sakata K, Okazaki K. Space charge polarization and aging of barium titanate ceramics. J Instit Electrical Engine Jpn. 1960;80:1460–1466.
[46] Schulthei J, Checchia S, Ursic H, et al. Domain wall-grain boundary interactions in polycrystalline Pb$(Zr_{0.7}Ti_{0.3})O_3$ piezoceramics. J Eur Ceram Soc. 2020;40:3965–3973.
[47] Li X, Cheng Y, Wang F, et al. Enhancement of energy storage and hardness of (Na0.5Bi0.5)0.7Sr0.3TiO3-based relaxor ferroelectrics via introducing Ba(Mg1/3Nb2/3)O3. Chem Eng J. 2022;431:133441.
[48] Chen Z, Liang R, Zhang C, et al. High-performance and high-thermally stable PSN-PZT piezoelectric ceramics achieved by high-temperature poling. J Mater Scien Technol. 2022;116:238–245.